Experimental and Numerical Kinetic Study of OME_1 and OME_2 Combustion in Low-Pressure Laminar Flame

Yanan Huo,* Véronique Dias, and Hervé Jeanmart

Institute of Mechanics, Materials and Civil Engineering (iMMC), Université catholique de Louvain, Louvain-la-Neuve, Belgium

Abstract

The combustion chemistry of OME_1 and OME_2 was studied in stoichiometric laminar flames at low pressure, 50 mbar, by carrying out flame structure measurements with molecular-beam mass spectrometry (MBMS). The kinetic modeling has been performed under the same conditions and the simulated results were compared with experimental results. A new detailed kinetic sub-mechanism for OME_2 will be developed and added to the previous UCL mechanism.

Introduction

The urgency of reducing the emission of greenhouse gases and achieving a circular carbon economy encourages research on renewable energy systems. The alternative synthetic fuels (e-fuels), produced from hydrogen and carbon dioxide (CO_2) via carbon capture and utilization (CCU) with renewable electricity, could be high-potential energy carriers for long-distance transportation and long-term storage [1][2]. Oxymethylene ethers (OME_s), formally known as polyoxyethylene dimethyl ethers (PODES), with structural formula of $CH_3O(CH_2O)_nCH_3$, is regarded as a potential asset to the current energy transition and one of the valuable candidates for e-fuels benefiting from its high energy density [3]. The absence of C-C bond and high oxygen content in OME_s bring enhanced efficiency and significant decreases in CO as well as soot emissions, without increasing NO_x emission when blended with diesel in the direct injection diesel engine [4].

Deep understanding of oxidation kinetics of OME_s remains a prerequisite for optimizing their combustion and for a comprehensive assessment of the engine application potential of OME_s in the future. As the simplest OME_s, the combustion kinetics of OME_1, which is also named as DMM, have been studied extensively with experimental and numerical methods [5–12]. Lean and rich premixed OME_1/oxygen/argon flames were studied in our previous work which resulted in a new sub-mechanism of OME_1 added into the UCL mechanism which includes the formation and consumption of oxygenated species involved in OME_1 oxidation [5]. Alzueta et al. [9, 10] investigated OME_1 oxidation in a flow reactor at high and atmospheric pressures, from fuel-lean to rich conditions. The study at atmospheric pressure [9], with the interpretation of their chemical kinetic mechanism, shows that methyl formate is a vital intermediate and the activation energy value of the reaction of methyl formate conversion to methanol and CO has a significant impact on modeling results. The soot precursor, acetylene, was only detected under pyrolysis and very reducing conditions. Few detailed studies have been conducted on longer-chain species (OME_n, $n>1$). The mechanism of OME_3 at low and intermediate temperatures for the prediction of the ignition characteristics was developed by He et al. [13] based on the reaction rates calculation with canonical transition state theory (CTST). Their mechanism has been validated against the results from RCM and HCCI experiments with good agreement. Cai et al. [14] investigated the ignition delay time of $OME_{2\text{-}4}$ in a shock tube. The chemical mechanism of $OME_{2\text{-}4}$ was obtained by using an automatic reaction class-based mechanism generator and was optimized automatically for higher prediction accuracy. Sun et al. [15] investigated the high-temperature combustion chemistry of stoichiometric OME_3 flat flame with a synchrotron vacuum ultraviolet photoionization mass spectrometry and measured the laminar burning velocities of OME_3/air mixture in a spherical bomb at atmospheric pressure. The reaction pathways analysis revealed that the absence of carbon-carbon bonds in the C-O chain structure is beneficial to soot-reduction and the relevant reaction patterns can ba applied to larger OME_s. In the recent work from Wang et al. [11], pyrolysis of $OME_{1\text{-}3}$ was studied in a jet-stirred reactor (JSR) at around atmospheric pressure (1.03 atm) and temperatures of 450-1080 K. The reactivity increases evidently with the increase of the fuel chain, reflected in the initial pyrolysis temperature decrease, which results from the production of CH_3 and H radicals from the unimolecular decomposition of $OME_{1\text{-}3}$. Methane and methyl formate were detected with high concentrations. Using JSR, they further investigated the low-temperature (500-950 K) oxidation kinetics of $OME_{1\text{-}3}$ [12]. It was found that, under low temperatures, OME_1 is directly decomposed into small molecules resulting in a faster decomposition rate than that of OME_2 and OME_3. Gaiser et al. [16] recently studied fuel-rich (equivalence ratio of 1.7) premixed flames of $OME_{0\text{-}4}$ with electron ionization (EI) MBMS at 40 mbar with the help of kinetic modeling with the

*Corresponding author: yanan.huo@uclouvain.be

mechanism from Kathrotia et al. [17] for interpretation, making conclusion that oxygenated species dominate the combustion process and the observed species pool is nearly independent of the chain length of the respective OME_s. The purpose of this work is to investigate the kinetics of OME_1 and to study the detailed combustion chemistry of OME_2 under low-pressure and stoichiometric conditions to understand the effects of ($-CH_2O$) chain length and be ready for the studies on higher OME_s in the future. The measurement and calibration of OME_1 stoichiometric flame has been performed. However, the calibration of intensity to mole fractions of species in OME_2 flame is in progress. This paper focuses on the investigation on detailed kinetics of OME_1 premixed flame.

Experimental methods

For the purpose of investigating the combustion chemistry of OME_s systematically, the MBMS flame setup was used for measurements of both OME_1 and OME_2 stoichiometric, premixed laminar flames at low pressures. Table 1 shows the inlet composition of flames. The argon and oxygen flow rates are controlled and metered by El-Flow mass flow meters from Bronkhorst (with an accuracy of ±0.5%). After being controlled and measured by the liquid Coriolis mass flow meter (Bronkhorst Mini Cori-Flow M12 with an accuracy of ±0.2%), the liquid fuel enters into a Controlled Evaporation Mixing (CEM) system from Bronkhorst, is evaporated and is mixed with the carrier gas argon. The flow rate of carrier gas was 2 L/min. The vaporizer temperature was set to 333.15 K for OME_1 and 383.15 K for OME_2. To prevent condensation, the gaseous mixture passes through a pipe, which is heated up to 473.15 K, and then is mixed with the rest of the argon and oxygen before entering the burner. The flames are stabilized at 50 mbar on a Spalding-Botha burner, 8 cm in diameter. The total flow rate of the inlet gaseous mixture is 5.72 slm. Parallel to the burner surface, a 2 cm length quartz cone (0.1 mm orifice) with a 45°angle allows direct sampling from the flame. Thanks to the mobility of the burner, samples can be taken at any point from the fresh gases to the flue gases, passing through the flame front. The range of height above burner (HAB) is 0-30 mm with a precision of 0.1 mm. The high vacuum chamber (10^{-5} mbar) behind the quartz cone forces the sampling gas to form a molecular beam, which is then sucked into the chamber of lower pressure (10^{-6} mbar), passes through a copper skimmer, and reaches the ionization chamber of the mass spectrometer (10^{-7} mbar). The axis of the mass spectrometer is perpendicular to the molecular beam. This arrangement allows the gaseous sample to be ”frozen”, which keeps chemical composition unchanged from the tip of the cone to the detection system and enables the detection of reactive chemical species avoiding reactions with other molecules or the wall. In order to minimize interferences either from fragmentation during the electron impact or from overlapping species with similar masses, the ionization potentials were measured and chosen specifically for the species detected with the precision of 0.01 eV. For OME_n (n>0), it is difficult to form stable molecular ions in the MBMS. The signal of molecular $C_3H_7O_2$ is regarded as OME_1, and of molecular $C_4H_9O_3$ is regarded as OME_2. The species measured in OME_1 and OME_2 flames are shown in the Table 2. Conversion of signal intensities to mole fraction profiles was performed using a calibrated mixture for stable compounds and estimating ionization cross-sections for radicals and unstable species. An internal calibration procedure was used for the calibration of the major species, such as OME_1, OME_2, O_2, CO_2, CO, H_2 and H_2O, with uncertainties lower than 6%. The direct calibration was used for the determination of CH_4 and C_2H_2 mole fraction profiles with uncertainties around 5-10%. Estimating ionization cross-sections for unstable species resulted in higher uncertainties (10-20%).

The flame temperature profiles will be obtained after all the measurements of stoichiometric $OME_{1\text{-}3}$ flames at the end. The one used for the simulations for the current procedure is based on the experimental temperature profile measured in the OME_1/O_2/Ar fuel-rich flame in [5].

Table 1: Stoichiometric flames inlet composition (slm at 273 K; 1013 mbar), with D_t (total flow rate), and italics in the brackets are mole fractions

	Fuel(g/h)	O_2(slm)	Ar(slm)	D_t(slm)
OME1	70 (*0.07*)	1.72 (*0.24*)	4.0 (*0.70*)	5.72
OME2	55 (*0.04*)	1.10 (*0.17*)	4.4 (*0.79*)	5.72

Numerical Modeling

In this work, two mechanisms were used for chemical kinetic modeling. The UCL mechanism was established by Dias et al. [5]. It has been developed to predict lean and rich premixed OME_1/O_2/Ar flames, and will be extended by building sub-mechanisms for OME_2 and OME_3 combustion. 480 elementary reactions and 90 chemical species are included in the UCL mechanism with detailed illustrations in the previous paper [5]. At the same time, the mechanism from Kathrotia et al. [17], which includes ethers from OME_0 to OME_5 with 1814 reactions and 238 species, was used for comparison with the OME_1 and OME_2 flames. It is named Kath-mechanism in the following discussion. The numerical modeling is performed using OpenSMOKE++ [18].

Results and Discussion

Figures 1-5 show experimental (symbols) and simulated (lines) mole fraction profiles of the chemical species measured. In the following section, we discuss the consumption of OME_1 and the formation of chemical species produced from OME_1. The primary and secondary radicals produced by H abstraction of OME_1

Table 2: Species measured in two flames and ionization potentials; IP-T:ionization potential threshold; IP: ionization potential used in the present work

Mass	Species	IP(eV)	IP-T(eV)	Flames
2	H_2	15.37	15.5	
15	CH_3	9.84	9.82	
16	CH_4	12.65	12.55	
18	H_2O	20.20	12.60	
26	C_2H_2	12.00	11.39	
28	CO	18.50	14.01	
28	C_2H_4	12.20	10.51	
29	HCO	9.84	9.84	
30	CH_2O	12.40	10.88	
31	CH_3O	11.68	11.67	
32	O_2	20.00	12.10	$OME_{1,2}$
32	CH_3OH	10.86	10.85	
33	HO_2	13.50	11.53	
34	H_2O_2	10.94	10.92	
40	Ar	26.00	15.90	
44	CH_3CHO	10.22	10.21	
44	CO_2	23.80	13.20	
44	C_3H_8	10.95	10.95	
45	CH_3OCH_2	9.13	9.11	
59	CH_3OCO	12.30	12.30	
60	CH_3CHO	10.82	10.81	
76	OME_1	20.00	10.38	
30	C_2H_6	11.55	11.55	OME_2
43	CH_3CO	8.10	8.05	OME_2
77	$CH_3OCH_2O_2$	10.00	10.59	OME_2
90	CH_3CH_2CHO	11.00	10.59	OME_2
106	OME_2	20.00	10.39	OME_2

are denoted as DMM_1 ($CH_2OCH_2OCH_2$) and DMM_2 ($CH_2OCHOCH_3$).

Figure 1 and Figure 2 present experimental and calculated mole fraction profiles of the reactants and products in the stoichiometric flame of $OME_1/O_2/Ar$ mixture. The results show a good agreement between experimental results and simulated ones from both mechanisms. In Figure 1, two mechanisms underestimated the mole fraction of O_2. The experimental results show that OME_1 was consumed earlier and faster than that estimated by the two mechanisms, probably caused by the shift of flames due to the sampling nozzle. In Figure 2, the mole fractions of the main products (H_2O, CO_2, CO and H_2) are shown. UCL-mechanism shows a good prediction of H_2O mole fraction starting position of around 5 mm. The experimental mole fractions of H_2 and CO are lower than the numerical results from both mechanisms. According to the research performed by Dias et al. [5] and Gaiser et al. [16], which showed the excellent prediction of the mechanisms, the deviation here might be from the estimated temperature profile used in the modeling for the current work. However, the two mechanisms show good agreement in the position of peak and trend along the distance from the surface of the burner. Unlike modeling results of the other three species, the mole fraction profile of H_2 from Kath-mechanism is higher than that from UCL-mechanism. From the results of simulations, H abstraction by OH and H dominates the consumption of OME_1. Among these, the reaction OME_1+H=DMM_1+H_2 shows the highest reaction rate in UCL-mechanism. However, the reaction OME_1+OH=DMM_1+H_2O is the fastest in the Kath-mechanism. The second most crucial consumption pathway for the UCL-mechanism is H abstraction by OH to produce DMM_1 and DMM_2, with identical reaction rates, followed by the reaction with the O. The reactions with H are the second most important consumption pathway in the Kath-mechanism. The last consumption of OME_1 is with CH_3 in both mechanisms.

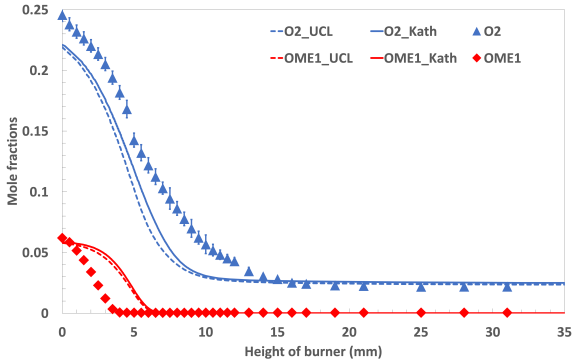

Figure 1: Experimental (symbols) and simulated (lines) mole fraction profiles of O_2 and OME_1

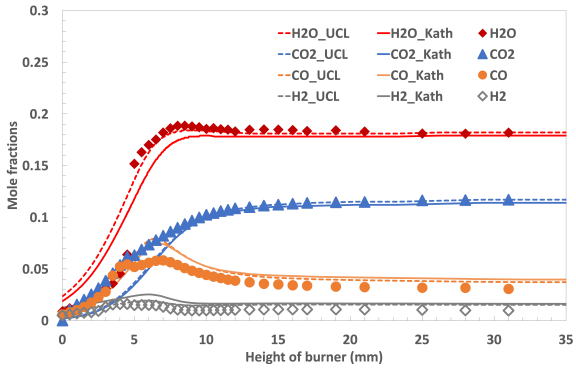

Figure 2: Experimental (symbols) and simulated (lines) mole fraction profiles of main products

Figure 3 shows the mole fraction profiles of CH_2O, CH_3 and CH_4 from experiments and simulations. A

good agreement of CH_4 mole fraction profile is observed between experimental results and numerical results from Kath-mechanism. The two mechanisms underestimate the mole fraction for CH_3 and overestimate that of CH_2O, but with good agreement on peak positions and trends.

Figure 4 shows the experimental and simulated mole fraction profiles of HCO and C_2H_2. With regard to HCO, the simulated results almost overlap with each other and underestimate the mole fraction of HCO on the peak position. The Kath-mechanism overestimates the concentration of C_2H_2, while UCL-mechanism underestimates it.

Figure 5 presents experimental and numerical results of C_2H_4 and HO_2. UCL-mechanism shows a good agreement on peak value against with the experimental mole fraction of HO_2 while the Kath-mechanism underestimates it. The apparent deviation of C_2H_4 from both simulated results is observed. It has been found that Kath-mechanism showed underestimation of C_2H_4 in work from Gaiser under fuel-rich OME_1 flame [16].

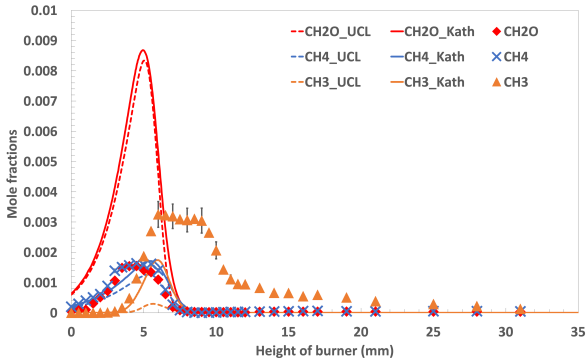

Figure 3: Experimental (symbols) and simulated (lines) mole fraction profiles of CH_3, CH_4 and CH_2O

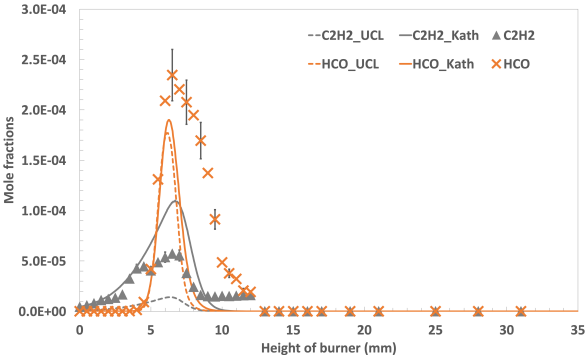

Figure 4: Experimental (symbols) and simulated (lines) mole fraction profiles of C_2H_2 and HCO

The two mechanisms were used to analyze the reaction pathway of OME_1 consumption and formation of essential intermediates, as shown in Figure 6. The bold black arrow line indicates the main pathway of OME_1 consumption in both mechanisms, which is similar to

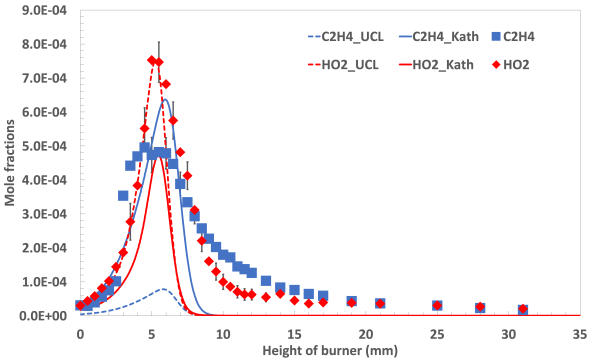

Figure 5: Experimental (symbols) and simulated (lines) mole fraction profiles of C_2H_4 and HO_2

the conclusion from our previous work on the fuel-rich flame of OME_1 [5]. The pathway of the dash line in red denotes the reactions that show more contributions in the UCL-mechanism while being less critical in the Kath-mechanism, and vice versa. The consumption reactions of HCO in UCL-mechanism might explain the lower predicted mole fraction of HCO, as shown in Figure 4. Similarly, the conversion of CH_3OCO to CH_3 might directly result in a higher simulated mole fraction of CH_3.

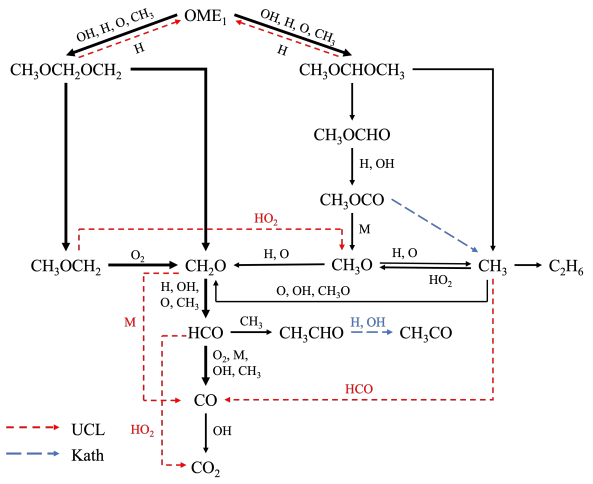

Figure 6: Reaction pathway of OME_1 consumption and formation of intermediates in stoichiometric $OME_1/O_2/Ar$ flames (solid black line: main and minor pathways in both mechanisms; short dash line in red: reactions only important in UCL-mechanism; long dash line in blue: reactions only important in Kath-mechanism)

Work in progress

The measurement of $OME_2/O_2/Ar$ stoichiometric flame is finished. Compared to the measurement of OME_1 flame, intermediates C_2H_6, CH_3CO, $CH_3OCH_2O_2$ and CH_3CH_2CHO were only detected in OME_2 flames, with specific ionization potentials in Table 2. The calibration is in progress. The new submechanism of OME_2 flame will be used for model-

ing, evaluated against the experimental results, and expanded to the combustion of OME_3. These results will guide future work on combustion chemistry OME_3 stoichiometric flame and $OME_{1\text{-}3}$ flames under fuel-lean conditions.

Conclusion

In this work, the stoichiometric flame of $OME_1/O_2/Ar$ and $OME_2/O_2/Ar$ were analyzed by molecular-beam mass spectrometry at 50 mbar. The mole fraction profiles of species, especially the reactive intermediates, were measured and presented. Numerical modeling was performed with UCL-mechanism and Kath-mechanism. The comparison of experimental results of OME_1 flame verified the experimental measurements and showed good agreement. From both mechanisms, OME_1 consumption is dominated by H-abstraction reactions. It follows two main pathways, with the first one being the fastest at the stoichiometric condition: $OME_1 \Rightarrow CH_3OCH_2OCH_2 \Rightarrow CH_3OCH_2 \Rightarrow CH_2O$ (Route 1) and $OME_1 \Rightarrow CH_3OCHOCH_3 \Rightarrow CH_3OCHO \Rightarrow CH_3OCO \Rightarrow CH_3O \Rightarrow CH_2O$ (Route 2).

Acknowledgements

The authors are very grateful for the financial support from Fonds de la Recherche Scientifique-FNRS under grant n°T.0119.21.

References

[1] K. De Ras, R. Van de Vijver, V. V. Galvita, G. B. Marin, and K. M. Van Geem, Carbon capture and utilization in the steel industry: challenges and opportunities for chemical engineering, *Current Opinion in Chemical Engineering* **26**, 81 (2019), ISSN 2211-3398, energy, Environment Sustainability: Sustainability Modeling Reaction engineering and catalysis: Green Reaction Engineering.

[2] L. E. Hombach, L. Doré, K. Heidgen, H. Maas, T. J. Wallington, and G. Walther, Economic and environmental assessment of current (2015) and future (2030) use of e-fuels in light-duty vehicles in germany, *Journal of Cleaner Production* **207**, 153 (2019), ISSN 0959-6526.

[3] Y. Fenard and G. Vanhove, A mini-review on the advances in the kinetic understanding of the combustion of linear and cyclic oxymethylene ethers, *Energy & Fuels* **35**, 14325 (2021).

[4] H. Liu, Z. Wang, J. Zhang, J. Wang, and S. Shuai, Study on combustion and emission characteristics of polyoxymethylene dimethyl ethers/diesel blends in light-duty and heavy-duty diesel engines, *Applied Energy* **185**, 1393 (2017), ISSN 0306-2619, clean, Efficient and Affordable Energy for a Sustainable Future.

[5] V. Dias, X. Lories, and J. Vandooren, Lean and rich premixed dimethoxymethane/oxygen/argon flames: Experimental and modeling, *Combustion Science and Technology* **182**, 350 (2010).

[6] W. A. Kopp, L. C. Kröger, M. Döntgen, S. Jacobs, U. Burke, H. J. Curran, K. Alexander Heufer, and K. Leonhard, Detailed kinetic modeling of dimethoxymethane. part i: Ab initio thermochemistry and kinetics predictions for key reactions, *Combustion and Flame* **189**, 433 (2018), ISSN 0010-2180.

[7] F. H. Vermeire, H.-H. Carstensen, O. Herbinet, F. Battin-Leclerc, G. B. Marin, and K. M. V. Geem, Experimental and modeling study of the pyrolysis and combustion of dimethoxymethane, *Combustion and Flame* **190**, 270 (2018).

[8] C. A. Daly, J. M. Simmie, P. Dagaut, and M. Cathonnet, Oxidation of dimethoxymethane in a jet-stirred reactor, *Combustion and Flame* **125**, 1106 (2001), ISSN 0010-2180.

[9] L. Marrodán, F. Monge, Ángela Millera, R. Bilbao, and M. U. Alzueta, Dimethoxymethane oxidation in a flow reactor, *Combustion Science and Technology* **188**, 719 (2016).

[10] L. Marrodán, E. Royo, Millera, R. Bilbao, and M. U. Alzueta, High pressure oxidation of dimethoxymethane, *Energy & Fuels* **29**, 3507 (2015).

[11] X. Zhong, H. Wang, Q. Zuo, Z. Zheng, J. Wang, W. Yin, and M. Yao, Experimental and kinetic modeling studies of polyoxymethylene dimethyl ether (pode) pyrolysis in jet stirred reactor, *Journal of Analytical and Applied Pyrolysis* **159**, 105332 (2021), ISSN 0165-2370.

[12] H. Wang, Z. Yao, X. Zhong, Q. Zuo, Z. Zheng, Y. Chen, and M. Yao, Experimental and kinetic modeling studies on low-temperature oxidation of polyoxymethylene dimethyl ether (dmm1-3) in a jet-stirred reactor, *Combustion and Flame* **245**, 112332 (2022), ISSN 0010-2180.

[13] T. He, Z. Wang, X. You, H. Liu, Y. Wang, X. Li, and X. He, A chemical kinetic mechanism for the low- and intermediate-temperature combustion of polyoxymethylene dimethyl ether 3 (PODE3), *Fuel* **212**, 223 (2018).

[14] L. Cai, S. Jacobs, R. Langer, F. vom Lehn, K. A. Heufer, and H. Pitsch, Auto-ignition of oxymethylene ethers (OMEn, n = 2–4) as promising synthetic e-fuels from renewable electricity: shock tube experiments and automatic mechanism generation, *Fuel* **264**, 116711 (2020).

[15] W. Sun, G. Wang, S. Li, R. Zhang, B. Yang, J. Yang, Y. Li, C. K. Westbrook, and C. K. Law, Speciation and the laminar burning velocities of poly(oxymethylene) dimethyl ether 3 (POMDME3) flames: An experimental and modeling study, *Proceedings of the Combustion Institute* **36**, 1269 (2017).

[16] N. Gaiser, H. Zhang, T. Bierkandt, S. Schmitt, J. Zinsmeister, T. Kathrotia, P. Hemberger,

S. Shaqiri, T. Kasper, M. Aigner, et al., Investigation of the combustion chemistry in laminar, low-pressure oxymethylene ether flames (ome0–4), *Combustion and Flame* 112060 (2022), ISSN 0010-2180.

[17] T. Kathrotia, P. Oßwald, J. Zinsmeister, T. Methling, and M. Köhler, Combustion kinetics of alternative jet fuels, part-III: Fuel modeling and surrogate strategy, *Fuel* **302**, 120737 (2021).

[18] A. Cuoci, A. Frassoldati, T. Faravelli, and E. Ranzi, Opensmoke++: An object-oriented framework for the numerical modeling of reactive systems with detailed kinetic mechanisms, *Computer Physics Communications* **192**, 237 (2015), ISSN 0010-4655.